Wear 274–275 (2012) 345–354

Contents lists available at SciVerse ScienceDirect

Wear

journal homepage: www.elsevier.com/locate/wear

Microstructures and abrasive wear performance of PTAW deposited Ni–WC overlays using different Ni-alloy chemistries

T. Liyanage [a], G. Fisher [b], A.P. Gerlich [a,*]

[a] University of Alberta, Chemical and Materials Engineering, Edmonton, Alberta T6G 2V4, Canada
[b] Alberta Innovates – Technology Futures, 250 Karl Clark Road, Edmonton, Alberta, T6N 1E4, Canada

ARTICLE INFO

Article history:
Received 21 April 2011
Received in revised form
29 September 2011
Accepted 10 October 2011
Available online 15 October 2011

Keywords:
Three-body abrasion
Hardness
Metal-matrix composite
Hardfacing
Mining
Mineral processing
Electron microscopy

ABSTRACT

The microstructures and performance of Ni–WC (nickel–tungsten carbide) composite overlays deposited by plasma transferred arc welding are studied using a combination of microscopy, hardness, and wear testing. The Ni–WC overlays had microstructures consisting of γ-Ni dendrites, with interdendritic Ni-based eutectics, borides and carbides. Overlays which were produced with a low hardness Ni-alloy matrix contained a smaller fraction of interdendritic phases relative to the high hardness Ni-alloys.

The dissolution of WC particles was observed following deposition of the MMCs, and this promoted the formation of secondary carbide phases. Ni-alloys with low carbon and low Cr content exhibited the least dissolution of WC. The Ni–WC overlays produced using these dilute alloys generally performed better in ASTM G65 wear tests. This was due to the increased fraction of retained WC phase, and the reduced fraction of brittle secondary carbide phases when the Ni-alloy contained no Cr.

1. Introduction

Overlay welding is used to improve the wear resistance of surfaces on industrial parts by depositing a protective layer of abrasion and/or corrosion resistant weld metal onto a base material surface. This technique is especially useful in high wear environments such as those experienced in a wide range of mining industries, in particular those encountered in the oil sands of Alberta. The extreme wear decreases productivity and the useful life of equipment, as such overlay welding is used to apply a thick coating onto components in order to reduce the overall maintenance costs [1–3].

The abrasive wear resistance increases strongly with the addition of tungsten carbide (WC) into the metallic matrix [2,4–8]. As a result, WC particles are an ideal candidate for addition into Ni-based alloys as the reinforcing phase since the low melting point of NiCrBSi alloys (about 1025 °C) allows tungsten carbide to endure the deposition process without degradation more readily than in Fe-based matrix alloys [9].

A central problem with plasma transferred arc welded (PTAW) Ni–WC overlays is the degree of dissolution of the WC particles [10]. Dissolution results in lowered wear resistance as there is less WC reinforcing material remaining to offer protection from abrasive wear [11]. In addition, the dissolved W, and C allow the formation of brittle secondary phases which may be detrimental to the abrasion resistance of the deposit [3]. Particle dissolution occurs when excessive arc current provides sufficient heat to cause WC material to go into solution above a critical temperature [12].

In order to prevent precipitation of brittle hard phases during laser welding, it was found that alloys with low contents of carbon, boron, and chromium should be used [13]. The diffusion coefficient of carbon in the matrix material is usually higher than the diffusion coefficient of the carbide-forming metal [14]. Thus, carbon diffuses much faster out of the carbide, allowing it to form mixed carbides. Complex carbides such as the metastable and extremely brittle η phase M_3W_3C form in MMCs due to the low carbon concentration in matrix alloys and the rapid cooling of the melt when WC is used as reinforcing particles [13]. Laser cladding of a NiCrBSi alloy with WC particles resulted in a matrix microstructure similar to that processed with no WC particles present, since the dissolution of WC particles is very low (~5%) using the laser cladding process [15]. The matrix was composed of γ-Ni dendrites and γ-Ni + Ni_3B lamellar eutectic in the interdendritic region. Blocky precipitates formed both near and away from the WC-matrix interface were found to be β-W_2C and contained some Cr. Quadrilateral precipitates were found to be η_1-M_6C with some Cr and Ni (possibly $(Cr,Ni)_3W_3C$) and thin-plate carbides were reported as α-W_2C [15]. In addition,

* Corresponding author. Tel.: +1 780 492 8853; fax: +1 780 492 2881.
E-mail address: gerlich@ualberta.ca (A.P. Gerlich).

0043-1648/$ – see front matter.
doi:10.1016/j.wear.2011.10.001

in the interface between WC particles and the matrix, M_6C tends to form as well as small fractions of Fe_3W_3C [16]. Away from the WC/matrix interface, more complex carbides have also been found in NiCrBSi alloys containing W; their chemistry was suggested to follow the formula $(NiSi)_A(CrW)_B$, with A and B taking values in the ranges (2.5–2.9) and (2.5–3.6), respectively [16].

The secondary particles resulting after WC dissolution occurs may produce Cr_7C_3, secondary tungsten carbide W_2C and metallic tungsten (W), Cr_3Ni_2, and $Cr_{23}C_6$, and these have been readily observed by XRD following thermal spray deposition of a low chromium NiCrBSi alloy with WC particles [17]. Laser cladding of spherical WC particles with a Ni-alloy also showed XRD peaks corresponding to γ-Ni, WC, W_2C and WC_{1-X}, Ni_2W_4C and CrFeNi [18]. When PTAW was used to deposit two NiCrBSi alloys with WC hard particles, dissolution of WC was evident due to the presence of elongated precipitates rich in W next to the WC particles and a small concentration of W in solid solution [3]. Dissolution of WC carbides also was noted using similar methods during laser cladding of another MMC (75% Ni–25% WC) alloy [19].

It is important to consider the formation of these phases in the matrix, since during abrasive wear the surface of a soft material is gouged out by the abrasive particles/phases of the harder material and produces wear chips when the abraded material is elastoplastic or viscoelastic-plastic. Abrasive wear involves subsurface plastic deformation (increases as wear particles themselves develop flat surfaces) in addition to cutting of the surface and generation of wear chips [20].

It is generally understood that increasing the hard particle fraction will increase coating hardness and hence abrasive wear resistance. It was found that for laser deposited Ni-based alloys with WC particles, increasing the WC volume fraction from 0 to ~50% did indeed show a linear dependence of hardness on the concentration of carbides but there was no correlation with the size of the particles [4]. Ball-on-disc wear testing showed that smaller carbides were more effective for dry sliding wear resistance since coatings with large carbides revealed evidence of cracks at the interface between carbides and matrix [4]. The effect of morphology of the WC particles (spherical or angular) on wear rate has also been compared, and the ASTM-G65 dry sand rubber wheel apparatus test reveals that MMCs with angular WC powder exhibit up to 50% lower wear rates than those obtained with spherical powder. It was argued that the surfaces of the clad layer formed with spherical powder had large gaps between reinforcing particles whereas with the angular powder, the particles formed an interlocking structure, exposing less of the matrix material to the abrasive particles [18]. This implies that the mean free distance between WC particles also plays an important role in wear resistance, where any dissolution of the WC material will be detrimental to the performance.

To assess the wear performance and carbide dissolution of Ni–WC composites during PTAW, three commercially available matrix alloys were tested with and without WC reinforcing particles. The matrix alloys differed in their compositions and could be categorized as being Cr-free, low-Cr, and high-Cr. These chemistries were chosen in order to compare the effect of alloying elements on the dissolution of carbides and their wear performance as MMCs.

2. Materials and methods

The matrix alloys used were two NiCrBSi powders and one NiBSi powder with compositions shown in Table 1. The WC powder used consisted of angular, monocrystalline particles (without any W_2C) with a size distribution of 50–180 μm and average of 100 μm. The MMC powders were mixed as 500 g batches (for each alloy) to a ratio of 60 wt% monocrystalline WC with 40 wt% Ni-alloy (which is approximately 50 vol%). Powders were mixed on a tumbler for a minimum of 2 h and the mixed powders were poured directly from the tumbler into the PTAW system hopper to be welded (i.e. without storing between mixing and welding) to minimize any settling of the dense WC particles.

Table 1
Matrix alloy element compositions (in wt%).

	B	C	Cr	Fe	Ni	Si
Alloy A (Cr-free)	3.45	0.027	0.16	0.64	92.64	3.08
Alloy B (low-Cr)	1.93	0.67	8.39	5.2	79.79	4.02
Alloy C (high-Cr)	2.73	0.92	13.8	5.5	71.25	5.8

The MMC overlays were applied using a Stellite Starweld 300M constant current power source with a Stellite Excalibur PTA torch. The PTAW parameters were as follows: arc voltage of 25 V, current of 150–160 A (in DC electrode negative polarity), powder feed rate of 25–30 g/min, Ar gas shielding at a flow rate of 12 l/min, 14 mm working distance, and a travel speed of 0.3–0.5 mm/s. In order to compare the influence of the WC particles on the properties, the Ni-alloys were also deposited alone (without WC) using comparable PTAW parameters. The deposits were about 25–30 mm wide and about 4–6 mm in thickness.

2.1. Microscopy

MMC overlay deposits were cut (using a diamond reinforced cutting wheel) from the middle of the deposit and were then polished using standard laboratory techniques to a 1 μm finish. After polishing, optical microscopy was performed to quantify the WC fractions and examine some of the other phases in the matrix. Electron probe microanalysis (EPMA) with wavelength dispersive spectroscopy (WDS) was conducted using a CAMECA SX100 with a 20 keV accelerating voltage to map the elemental distribution in the deposits. Auger Electron Spectroscopy (AES) was also conducted using a JEOL JAMP-9500F instrument at an accelerating voltage of 15 keV to quantify the chemistry of phases contained in the deposits, and Ar ion sputtering was applied for 30 s prior to analysis to remove surface contamination. AES provides elemental quantification for small phases since it is a very surface sensitive technique (Auger electrons are emitted only from the first few nanometers of the surface), and consequently does not suffer from undesirable interaction volume effects observed with X-ray spectroscopy scanning electron microscopy (SEM) methods. In addition, AES is able to quantify the chemistry of lighter elements such as boron and carbon. Conventional SEM was then used to analyze the wear scars produced after abrasion testing. The volume fractions of WC and their mean free path in the composite overlays were calculated after examining at least 450 particles, over a region of at least 10.2 mm^2 in each Ni–WC overlay.

2.2. Hardness testing

Vickers microhardness testing was conducted using a Mitutoyo MVK-H1 indentation system, with a 25 g to 1 kg load and 15 s load time to determine the hardness of the matrix and WC particles, and this was complemented by Rockwell C testing to investigate the macro-scale hardness in the overlays. When analysis of specific phases was required, Vickers testing with a 25 load was used, however the average hardness of the matrix and WC particles in the composites could be obtained using 500 and 200 g loads respectively. The average hardness values are reported along with ±1 standard deviation, and the number of indents tested (n).

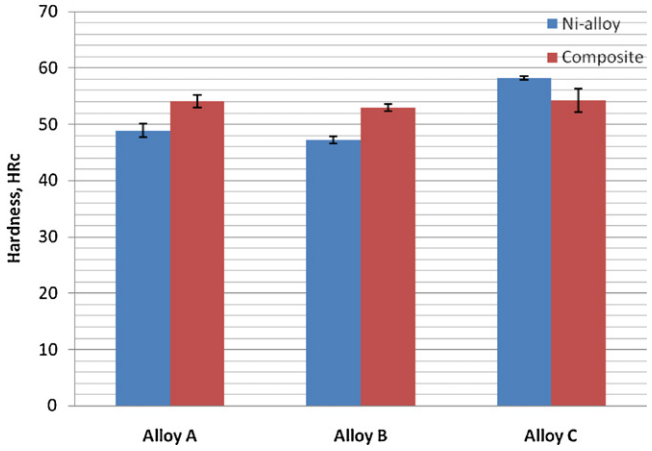

Fig. 1. Average hardness values of the Ni-alloy and Ni–WC composite overlays made using the different alloys studied.

2.3. Wear testing

Wear testing was performed as per the ASTM-G65-04 standard using Procedure A (dry sand rubber wheel apparatus), and the mass loss results were recorded for two consecutive wear scars (with 6000 revolutions of the abrasive wheel each) using a 130 N load on the wheel. Only the second wear scar mass loss values are reported, as the first scar generally involves preferential wear of the matrix during the so-called 'break-in' period. The abrasive used was Ottawa silica sand in a 50/70 mesh size (212–300 μm diameter particle size) with an angular morphology. Most deposits had a layer devoid of WC at the top of the deposit, and in order to avoid scatter due to the reduced WC fraction observed near the surface, samples were ground down by 1–2 mm to remove this region before wear testing.

2.4. Thermodynamic modeling

Thermodynamic modeling of the MMC system was performed using the ThermoCalc software package in order to compare the predicted phases expected to be stable with different alloy chemistries. A Scheil-type solidification model was applied in the TTNI8 database, with carbon as a fast diffuser and no bcc to fcc transformations. The results were then plotted as mass fractions of solid phases versus temperature. During calculation, it was assumed that the entire WC particle has initially dissolved (in order to represent the locally enriched region around the particles during partial dissolution), and the stability of various phases during subsequent cooling are compared using the Scheil plots for the three alloy chemistries studied.

3. Results

3.1. WC distribution and overlay hardness

Two major issues in achieving optimal performance of the Ni–WC composite overlays involve the non-uniform distribution and possible degradation or dissolution of the WC particles. All of the overlays contained a region devoid of WC at the top of the deposit as well as a higher density of WC particles at the sides of the weave weld. This inhomogeneity of the WC particles has been accounted for mostly by settling during the brief time that the overlay is fully molten [21].

The Rockwell C hardness values measured for the Ni-alloys and the Ni–WC composite overlays are compared in Fig. 1. The strengthening contribution of the WC particles is clear when Alloy A or B is employed, however the addition of WC particles did not have a significant contribution to the hardness of Alloy C. Vickers microhardness testing was also performed on the Ni-alloys with a 1 kg load at 250 μm intervals from the bottom (at the substrate/deposit interface) to the top of the deposit and compared to the hardness of the matrix alloy alone without WC particles. The trend in average Vickers microhardness through the thickness of the deposit centerline was comparable to the Rockwell hardness results.

When Alloys A, B, and C were deposited without WC particles, they exhibited hardness values of 529 ± 40 HV ($n = 25$), 503 ± 27 HV ($n = 15$), and 732 ± 62 HV ($n = 17$) respectively. Combining the alloys with WC particles slightly increased the microhardness of the alloy, where selective area measurements revealed that the metal matrix in the Ni–WC overlays made using Alloys A, B, and C were 617 ± 58 HV ($n = 20$), 601 ± 88 HV ($n = 20$), and 752 ± 100 HV ($n = 20$) respectively. The microhardness of the WC particles ranged significantly due to the anisotropy of the hexagonal crystal structure in the individual grains [22] and the average value was comparable in each of the composite overlays, being 1540 ± 242 HV ($n = 43$).

3.2. WC dissolution and microconstituents

Optical image analysis of the composite alloys (sections of low and high WC dissolution alloys are shown in Fig. 2a and b, Alloy A and Alloy C, respectively) was used to estimate the dissolution of the WC particles. Based on a 60/40 wt% ratio between WC/Ni-alloy, the volume fraction of the deposit should theoretically be 45 vol% WC–55 vol% Ni but 50 vol% WC was used for the purpose of dissolution calculations as some deviation occurs as a result of a minor difference in deposition efficiency of the materials (favoring WC). The highest dissolution was evident in the alloys which contained Cr and increased alloying elements. Most notably, the Ni–WC overlays produced using Alloy B and Alloy C which had high levels of Cr and C, exhibited high dissolution levels with more than 26% of the original WC material dissolving. No direct correlation could be determined between dissolution and specific alloying additions, since both the Cr and carbon content of each alloy increased in a roughly equal proportion.

Cross-sections were examined from the middle of the deposit to ensure consistency and to lessen any microstructural differences due to starting and ending the weave weld. The total WC fractions measured for each Ni–WC overlay are compared in Fig. 3, with a total of 10.2 mm^2 being examined for each value. However, it should be noted that along the length, some heating of the substrate will occur during preparation of the sample due to the slow travel speeds used. To take into consideration any scatter in the dissolution rate along the deposit length, sections were also made at the start, middle, and end of Alloys A and C. It was found that the difference in WC fraction calculation varied by 2–8% from the start to the end of the deposit. This suggests there was relatively little variation in the WC dissolution along the length of the deposit which could stem from the accumulation of heat in the substrate coupon during welding.

EPMA analysis revealed dissolution of primary WC carbides occurs and leads to the formation of secondary carbides surrounding the WC particles. Alloy A showed negligible dissolution with only some of the matrix appearing slightly enriched in tungsten (Fig. 4). A feathery Cr–W–C phase formed at the periphery surrounding the WC particles in Alloy B (Fig. 56) and AES element quantification (Table 2) of this phase suggested that the stoichiometry corresponds to $Cr_7W_3C_6$. The AES points analyzed in Alloy B are indicated in Fig. 6.

The Ni–WC overlay produced using Alloy C (which contained the highest fractions of Cr, C, and Si) contained blocky Cr–Ni–Si–W–C phases located between the WC particles (Fig. 7). Repeated AES element quantification of points in Fig. 8 revealed the stoichiometry

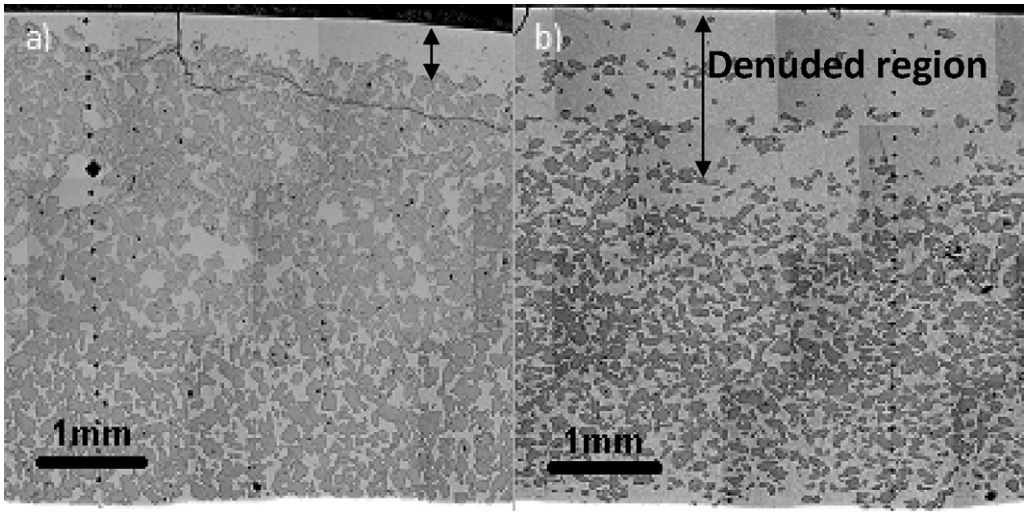

Fig. 2. MMC cross-sections illustrating examples of (a) low dissolution of WC when using Alloy A and (b) high WC dissolution when using Alloy C.

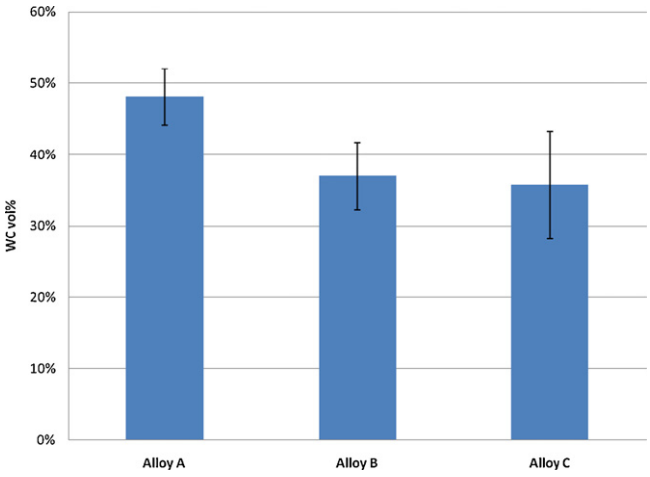

Fig. 3. Total WC fraction in Ni–WC overlays.

of the blocky 5-component phase to be about $Ni_4Cr_5Si_2W_4C_{4.5}$ as indicated in Table 3, although there may be some error in the C quantification due to some preferential removal of lighter elements during ion sputtering of the surface prior to collecting the AES data.

Microhardness testing was performed on the blocky 5-component phase observed in Alloy C (see Fig. 8) in order to determine its contribution to the overall hardness of the composite. Using a 25 g load, the average hardness of this 5-component phase was found to be 1570 ± 266 HV ($n = 17$), compared to 1540 ± 242 HV ($n = 43$) for the WC particles. One would expect that this blocky phase would make a significant contribution to the matrix hardness, however, only a marginal increase the microhardness of the metal matrix was oberved in Alloy C when this phase formed in the presence of WC particles (732 vs 752 HV). It should be noted that indents on the blocky 5-component phase using loads higher than 50 g consistently resulted in cracking of the phase, suggesting these are particularly brittle. When the regions adjacent to the Rockwell indents were examined, widespread cracking of the 5-component phases was observed in Alloy C (see Fig. 9), while negligible cracking was detected in the matrix of the Ni–WC overlays made using Alloy A or B. This provides strong evidence that this 5-component phase is likely more brittle than WC particles (only one of which contains a crack in Fig. 9 for example). This has drastic implications for the wear resistance of this Ni–WC overlay made using Alloy C. It should also be noted that extensive formation of slip bands were observed in the WC particles closer to the indent, which is a form of ductility widely observed in this carbide [22]. Due to the irregular crack paths at the Vickers indents, the toughness of the different phases could not be estimated directly from the crack lengths.

3.3. Wear testing results

Wear testing as per ASTM-G65 on the matrix alloys indicated that wear resistance correlated almost directly with hardness for each of the Ni-alloys, and the values were roughly in proportion to the measured hardness values (Fig. 10). In the case of the MMC wear performance, the overlays produced with matrix alloys with the lowest hardness, actually yielded the best wear resistance, as indicated in Fig. 11

Table 2
Repeated AES quantifications of the 3-component phase at the periphery regions of WC particles in Alloy B (the analysis points are shown in Fig. 6).

Point	Atomic concentration (%)		
	C	Cr	W
1	37.2	43.9	17.3
2	36.6	46.9	16.5
3	34.5	40.3	14.6
4	37	44.6	18.4
Average	36.32	43.92	16.7
Stoichiometry (est.)	6	7	3

Table 3
Repeated AES quantifications of the 5-component blocky phase between WC-particles in the Ni–WC composite produced using Alloy C (the analysis points shown in Fig. 8).

Point	Atomic concentration (%)				
	C	Cr	Ni	Si	W
1	21.6	26.6	20.9	11	19.9
2	21.5	25.4	21.1	9.1	22.9
3	22.6	24.4	21	12	20
4	22.4	24.2	20.2	10.4	22.8
5	24.1	26.3	20.2	9.9	19.5
6	22.3	26.6	21.6	11	18.5
7	23.3	26.5	21.1	9.8	19.3
8	22	26.7	20.5	12.2	18.6
Average	22.5	25.8	20.8	10.7	20.2
Stoichiometry (est.)	4.5	5	4	2	4

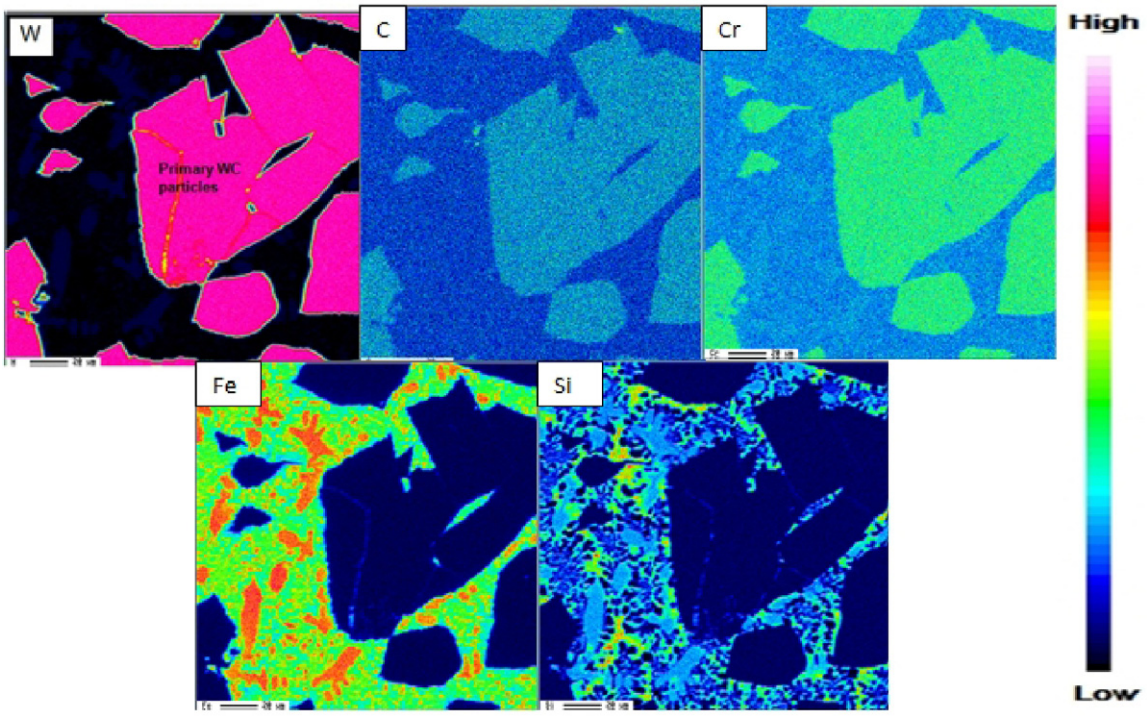

Fig. 4. EPMA element maps of Alloy A with WC particles.

. It is interesting to note that the wear rate drastically increases when the mean free path exceeds a critical value above 114 μm observed in Alloy B. The mean free path for the Ni–WC overlay produced using Alloy C was 129.5 ± 60 μm, which indicates that a significant fraction of the metal matrix on the surface of the wear scar can be in direct contact with the 212–300 μm diameter silica sand particles.

The wear scars examined by SEM imaging show that the WC particles are mostly intact and protrude above the metal matrix. In the case of the Ni–WC utilizing Alloy A, the surface of the WC particles is flat and smooth, with a short mean free path between adjacent WC particles (Fig. 12a). For Alloys B and C, the WC particles have a wider spacing due to increased dissolution and have a fractured, rough surface appearance (Fig. 12c). The wider separation between WC particles would

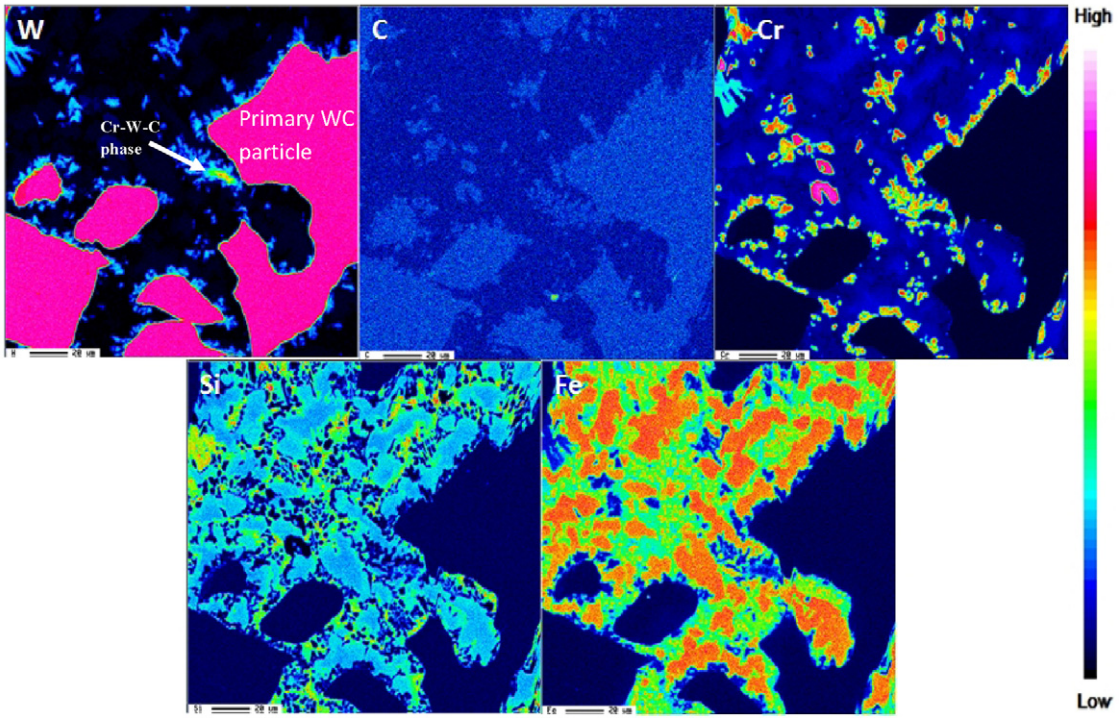

Fig. 5. EPMA element maps for W, C, Cr, Si, and Fe in Alloy B, showing the Cr–W–C rich phases at the periphery of the WC particles.

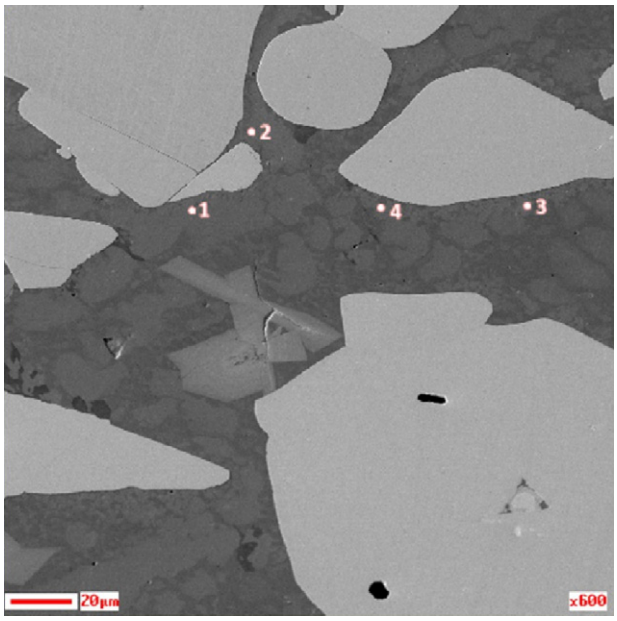

Fig. 6. SEM image of Alloy B containing the secondary phase involving C, Cr, W.

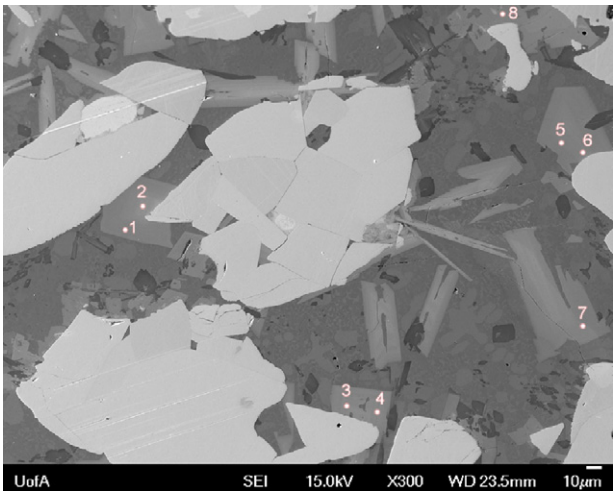

Fig. 8. SEM image of Alloy C composite containing the secondary blocky phase involving Cr, Ni, Si, W, and C.

allow more of the matrix to be worn away, accounting for the poor wear resistance observed in the Ni–WC based Alloy B and Alloy C.

3.4. Thermodynamic modeling

In order to account for the differences in the WC fractions and its effective dissolution tendency, thermodynamic modeling was performed on the three alloy systems and the results are shown for Alloys A, B, and C in Fig. 13, Fig. 14, and Fig. 15, respectively. The Scheil plots suggest that WC will actually reprecipitate during solidification if all of the WC has dissolved during deposition. Each Scheil plot indicates that solidification begins with WC phase ("FCC_A1#2" in the figures), followed by the formation of secondary carbides, borides and silicides along with the primary Ni-dendrites (FCC_A1#1 in the figures). The amount of these secondary carbides and borides increases from Alloy A through Alloy B, to Alloy C, and this is expected as the amount of alloying additions of C, B, and Si is increasing as well. These alloying additions form Cr-carbides and Cr-borides as well as other phases such as Ni-borides and Ni-silicides [23]. It is apparent that the WC phase (FCC_A1#2) is stable to a lower temperature before solidification of the Ni-dendrites in Alloy A compared to Alloy B or C. This suggests that during solidification of the MMC, the WC will be most stable in the chemistry of Alloy A during deposition, and least stable in Alloy C.

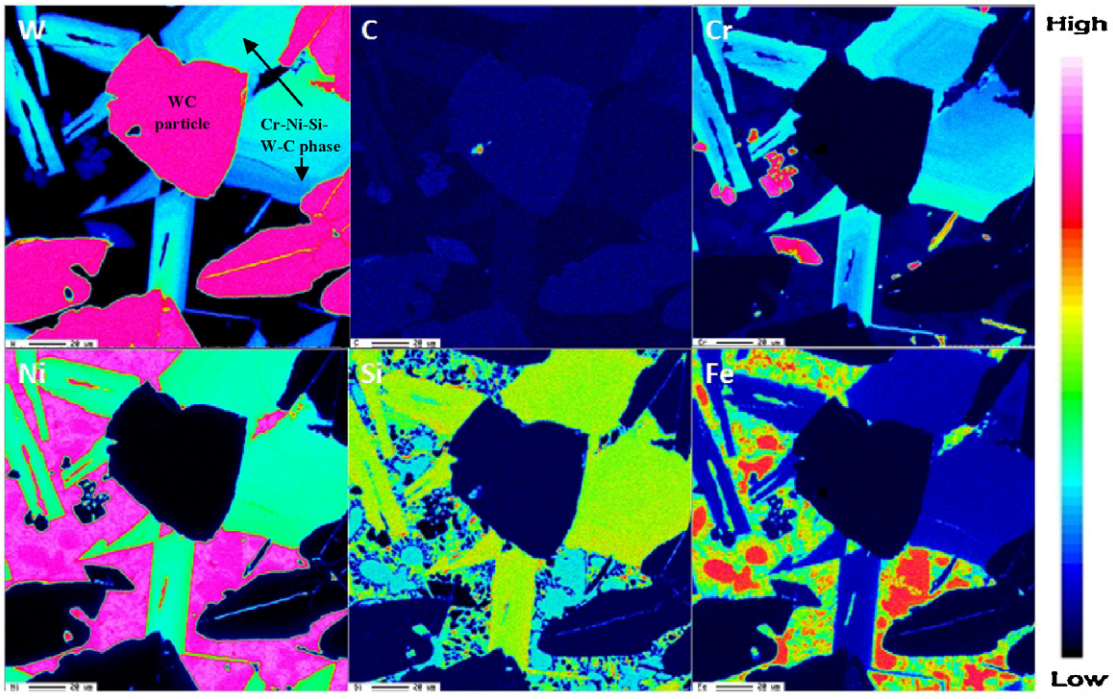

Fig. 7. EPMA element maps of W, C, Cr, Ni, Si, and Fe the Ni–WC composite utilizing Alloy C which contained the blocky Cr–Ni–Si–W–C phase.

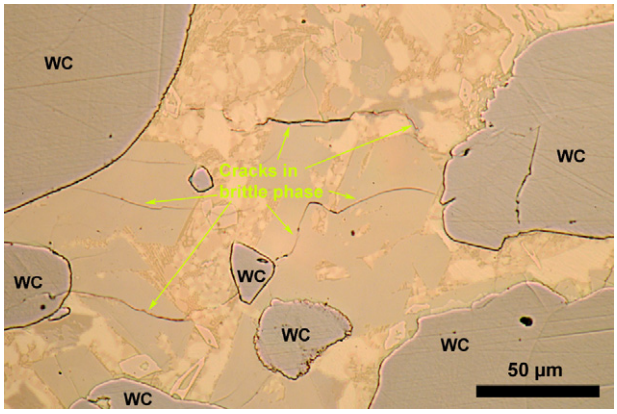

Fig. 9. Extensive cracking of the Cr–Ni–Si–W–C blocky phase observed adjacent to a Rockwell indent in the Ni–WC composite utilizing Alloy C.

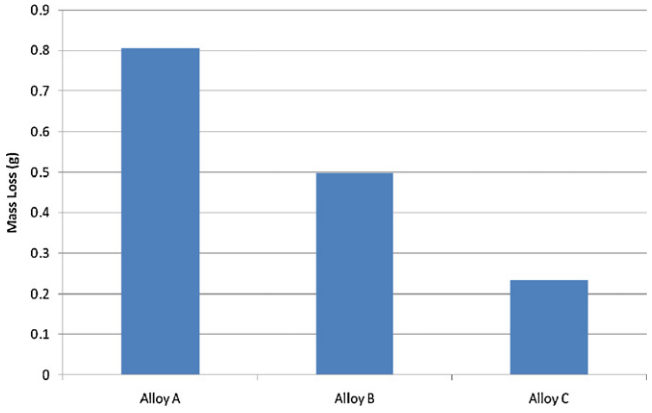

Fig. 10. ASTM-G65 wear results for the Ni-alloys tested (wear results are for the second wear scar).

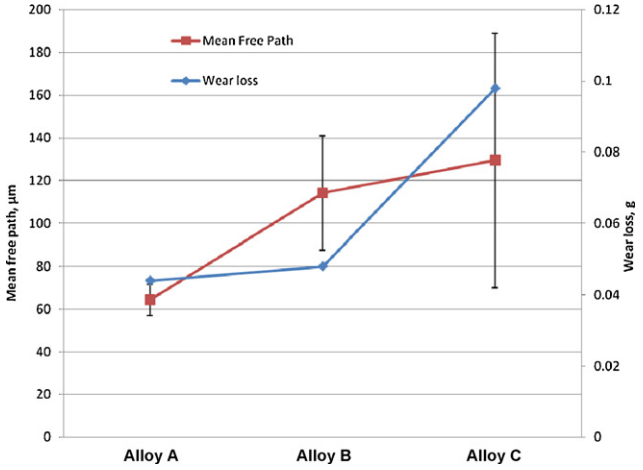

Fig. 11. Mean free path between WC particles, and ASTM-G65 wear results for the Ni–WC overlays (wear results are for the second wear scar).

4. Discussion

4.1. Microstructure

Dissolution of the primary tungsten carbide particles was clearly observed after PTAW and this resulted in the formation of secondary phases bearing W, C, Cr, as well as Ni and Si when the chemistry increased in Cr and Si. Alloy A contained very few secondary phases formed from dissolved WC since the dissolution was limited to less than 4%. Some phases also appeared to be slightly enriched in W that also contained Fe, and Si in solution. These phases containing Fe and Si were found in the MMC overlay involving Alloy A, and suggesting they have a high affinity for dissolved tungsten in the composite alloys. The secondary phase contained

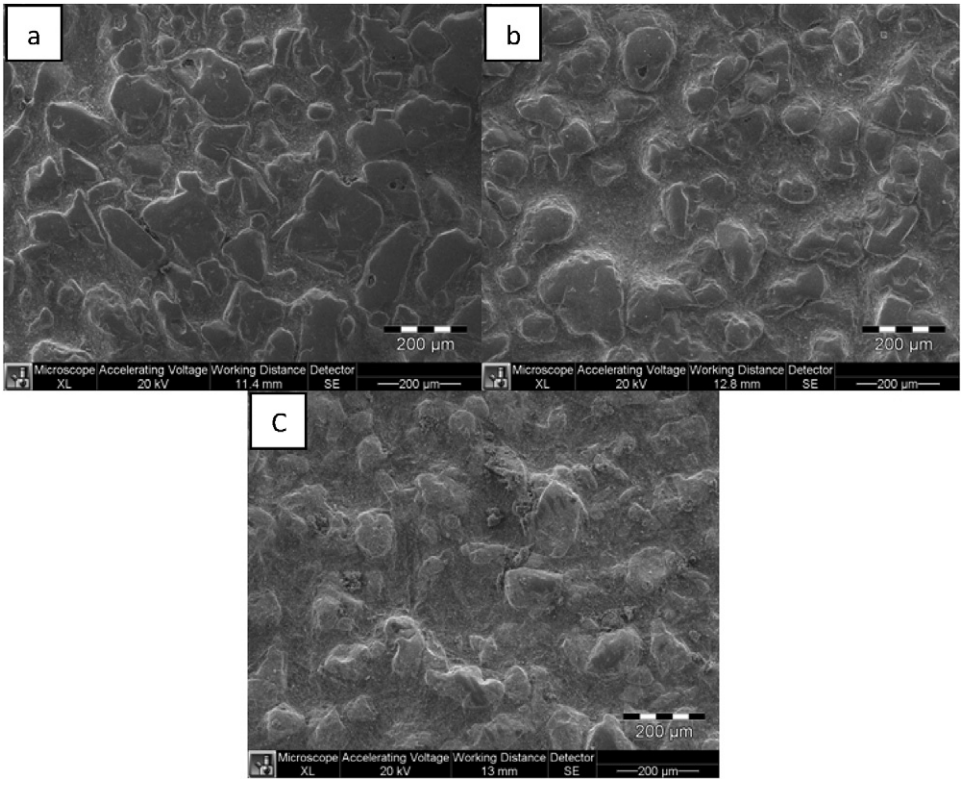

Fig. 12. Wear scars for Ni–WC composites utilizing (a) Alloy A, (b) Alloy B, and (c) Alloy C.

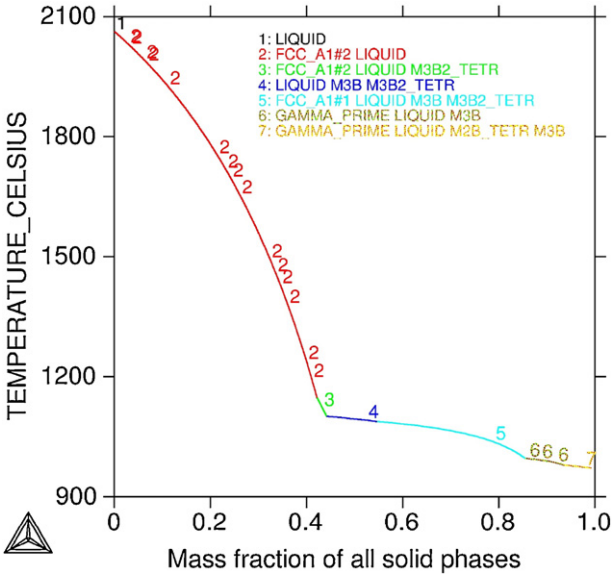

Fig. 13. Calculated Scheil plot for Alloy A.

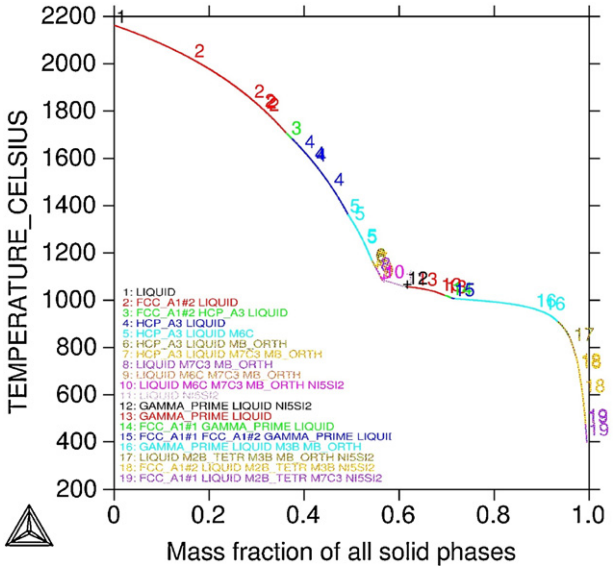

Fig. 15. Calculated Scheil plot for Alloy C.

Cr, W, and C in the case of Alloy B and formed at the periphery outlining the primary tungsten carbides and was quantified by AES to be about $C_6Cr_7W_3$. Based on the C–Cr–W ternary phase diagram, the intermetallic phases expected in this system are C_3Cr_6W, $C_4Cr_2W_3$, and possibly C_3Cr_5W. Although there may be some inaccuracy in the quantification of carbon which makes it difficult to verify which of these ternary phases are actually observed, the ratio of Cr to W is not consistent with the equilibrium phases. Consequently, it is possible that the observed C–Cr–W ternary phase is a non-equilibrium (meta-stable) precipitate. It is not likely that this is actually a M_7C_3, where M is comprised of Cr or W since the C–Cr–W ternary particle was observed in both Alloys B and C.

In the case of Alloy C, the secondary phases formed a large blocky phase and contained Cr, W, C, Ni, and Si. A similar W–Cr–Ni–Si phase was also detected in the case of Ni–WC overlay deposits made using gas metal arc welding, however, carbon may not have been detected in that study due to the use of EDX which is not sensitive enough to quantify C without significant error [21]. In addition,

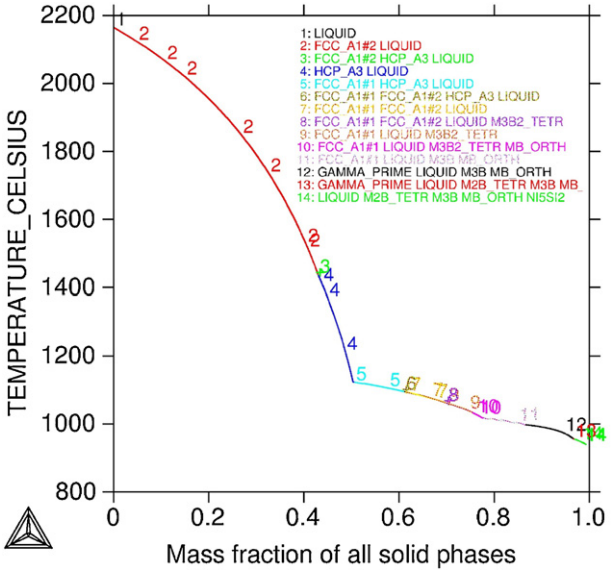

Fig. 14. Calculated Scheil plot for Alloy B.

laser remelted NiCrBSi + WC alloy analyzed by EDS also revealed that some secondary phases had W, Ni, Cr, Si as well as possibly other elements that were not reliably detected by EDS [7]. Using AES however, this blocky secondary phase was quantified and found to have a stoichiometric formula of about $Ni_4Cr_5Si_2W_4C_{4.5}$. It should be noted that although this phase appears to nucleate from the WC particles in the micrographs, is more likely to have grown from liquid phase in between the WC particles during solidification, since these are rather coarse and the time for solid state nucleation and growth is limited during cooling. Based on the morphology and small gradients in the chemistry across these particles, it appears these have grown as single crystals. Evidence of this is visible in the EPMA map of W in Fig. 7 where there appears to be segregation of elements outward from a central point which is away from the WC particle, and the gradient in W chemistry follows the angular geometry of the particle boundary. Similarly, fine dendrites in the matrix of other Ni–WC composites were attributed to the formation of numerous primary mixed carbides in the melt which then provided heterogeneous sites for the nucleation of the γ-nickel phase [24].

In comparison, when several Ni-base alloys with WC particles were deposited by laser on steel substrates so that the weld pool surface exceeded 3273 K and the alloy/substrate temperature was about 1788 K, very little dissolution of the WC particles was observed however they would dissolve completely if the W and C concentrations in the bulk alloy are reduced [12]. Thermodynamic calculations suggested that the terminal solidification temperature would be about 1617 K and could contain austenite, WC particles, and graphite once solidified. It was also suggested that at slower laser traveling speeds, enrichment of the interparticle region with carbon from dissolved WC results in the eutectic formation of austenite and carbide from liquid [12].

4.2. Hardness and wear resistance

The average Rockwell hardness of alloys A and B increased due to the fraction of WC reinforcing particles in the deposited overlay, however that of Alloy C actually decreased marginally when WC was present. However, one should consider that the volume fraction of WC was much lower when using Alloy C, and that when the alloy is deposited it contains a large fraction of Cr-borides and Cr-carbides which have hardness values ranging from 1250 to 2300 HV

[23], some of which are harder than WC. Hardness testing of Alloy C also revealed that the blocky secondary phases formed only when WC is present were brittle and promoted surface cracking, and this may contribute to the lower Rockwell hardness value observed in the composite.

In an abrasive wear situation, the load is transferred mostly to the reinforcing particles since any of the softer matrix phase between particles would either be gouged out or plastically deform away from the abrading surface/particles [7]. If the hard phase structures in the composite coatings form a load support system, it limits the amount of stress imposed on individual particles and hence ensures the particles are not at their mechanical and adhesive limits [7,25]. When a particularly hard matrix material is used, it may not be able to absorb energy during impacts with the larger abrasive particles [26] and this leads to chipping and accelerated removal of the matrix. This can ultimately lead to the reinforcing particles decohering from the matrix and being removed.

The relative size of abrasive particles to the reinforcing particles and their spacing in the metal matrix of an MMC also has an influence on wear resistance. Wear in the 3-body loading situation during ASTM G65 testing mainly results from the loss of matrix when the abrasive particles are small (low stress abrasion), while it could result more from microcracking and particle pull-out when the abrasive particles are large (high stress abrasion) [26]. However, a size ratio around 1:1 (for the reinforcing particle relative to the abrasive particle) could facilitate the penetration of the abrasive particles into the matrix to damage both the matrix and the reinforcement, thus enhancing the wear attack [26]. For the alloys examined, the WC particles were up to 180 μm in size with an average size of 100 μm and the sand particles were between 212 and 300 μm, and so the WC particle size versus abrasive size ratio ranges from approximately 1:1 to 1:2. As such the mechanisms of matrix damage, microcracking, and particle pull-out were expected to be the major causes of wear, although little evidence of particle pull-out was found in this study.

In the case of Ni–WC deposits which exhibited a high level of WC dissolution (e.g. Alloy C), there is a higher mean free path (129.5 ± 60 μm) between particles. Considering the sand size used, it is possible for silica abrasive to fit between the WC particles and readily gouge out the metal matrix. Fig. 11 shows a direct correlation between the mean free path (between WC particles) and the wear rate, in which the wear rate dramatically increases when a critical mean free path is exceeded (Alloy C). The much wider standard deviation observed in the mean free path observed when using Alloy C results in a far greater surface area of the matrix material being exposed to the sand particles. Considering the geometry aspect of the mean free path, coupled with the fact that the matrix material in the Ni–WC composite made using Alloy C contained a large volume of the brittle 5-component phase (demonstrated by Fig. 9), it is not surprising that its wear rate was so drastically higher.

Another aspect of abrasive wear in these composites is that once a portion of the matrix is removed, the sand is also able to slide between and impact the sides of the WC particles, leading to shear loads being imposed on the WC particles which promoted fracture as shown in Fig. 12c. Shear loading is detrimental to the WC particles, leading to increased fracture since ceramics generally perform better under compressive loads. This explains why Ni–WC overlays that exhibit higher WC dissolution did not perform as well as those experiencing minimal WC dissolution. Chipping of the WC particle edges can occur in all overlays regardless of WC dissolution, however it was clearly more prevalent when the dissolution is high based on the surface appearance of the WC particles in Alloy C.

The toughness of the overlays has some influence on the wear resistance, particularly in high stress abrasion since the formation of ductile primary Ni-dentrites in the matrix allows the overlay to plastically deform and absorb impact during abrassive wear. The overlays produced with a high hardness metal matrix have a lower fraction of primary Ni-dendrite, and mainly comprise brittle interdentritic phases which reduce the potential impact absorption. For example, it is worth noting that the uppermost crack highlighted in Fig. 9 propagates throught the brittle 5-component phase, however the primary Ni-dendrites to the left of this phase are not cracked and have obstructured the crack path. The more abundant interdendritic material undergoes brittle failure and is worn away to expose the edges of the WC particles to impacts by the abrasive media.

It has been suggested that secondary phases which form as a result of dissolution around the reinforcing WC phase aid in wear resistance as they bind the WC particles more strongly to the matrix and prevent particle pull out [14,27]. However, analysis of wear scars by SEM did not show evidence of particle pull-out in the wear scars examined for any of the overlays examined. As such, the reinforcement-matrix interface strength does not appear to have a major influence on the wear performance in the MMC deposits considered in this study.

4.3. Thermodynamic modeling

Thermodynamic modeling of the alloy systems suggested that the stability of the WC phase was reduced as alloying elements (particularly Cr) was increased in Alloys B and C, and this correlated well with the WC fraction measurements. Dissolution of WC particles was highest in the Cr-containing alloys (B and C) and is likely a result of: (a) WC being stable down to a lower temperature in the Cr-free alloy, (b) the WC starting to solidify at a lower temperature in the Cr-free alloy, and (c) the precipitation of high melting temperature phases such as Cr-carbides and Cr-borides being preferred over WC. The reprecipitation of WC was also predicted to occur at 1844 K in recent ThermoCalc modeling of the laser cladding process [12].

In the Cr-free alloy, WC as well as the primary Ni-dendrites start to solidify at a lower temperature, which facilitates the application of lower heat input values into the weld and reduces the dissolution. Solidification continues to a lower temperature in Alloy A compared to Alloys B and C, along with less competition for the carbon to form from other carbides. In the case of Alloys B and C, there are many more high melting temperature phases incorporating carbon, boron, and silicon relative to the Cr-free alloy, and this results in an increased solid fraction that may require higher heat input needed to maintain a low viscosity weld pool during welding. It was noted that the higher Cr content alloys were more difficult to promote wetting with the steel substrate during deposition.

Based on the observed results, the fundamental issue which leads to severe wear in WC composite overlays is the replacement of WC by other carbides or phases with inferior properties. This is predicted by the thermodynamic modeling, which shows that the temperature range for stability of the WC is reduced when alloying additions such as Cr and Fe are made to the Ni-alloy matrix, which reduces the volume fraction of WC in the overlay and promotes formation of brittle phases in the metal matrix.

5. Conclusions

The Ni–WC composite overlays examined showed similar microstructures and phases to that of the matrix alloys, however there were also other secondary phases that formed during deposition as a result of WC particle dissolution. A Cr-free alloy (Alloy A) exhibited little dissolution of WC, while the addition of approximately 8% Cr to the matrix (Alloy B) promoted dissolution of WC and the formation of small secondary carbides (approximately $Cr_7W_3C_6$). When high values of Cr are added to the matrix alloy

(nearly 14% in Alloy C), significant fractions of brittle secondary carbides with stoichiometry around $Ni_4Cr_5Si_2W_4C_{4.5}$ were precipitated after WC dissolution.

The average Rockwell hardness of the Ni-alloys increased more significantly with the addition of WC particles when the Ni-alloy initially has a hardness <50 HRc. In terms of wear loss, the MMC overlays were from two to five times more wear resistant than the matrix alloys without the WC particles. The MMCs with the softer matrix alloys generally performed better than those with hard matrix alloys. It is suggested that this is due to the presence of brittle secondary phases, less energy absorption by the matrix, and a larger mean free path between WC particles (due to dissolution) in the MMC overlays when Cr-rich Ni-alloys are used. Particle pull-out, which has been observed in previous studies, was not widely observed in the wear samples examined.

Acknowledgements

The authors wish to thank the support of the Natural Sciences and Engineering Council (NSERC) of Canada, and the Alberta Energy Research Institute (AERI).

References

[1] D.J. Branagan, M.C. Marshall, B.E. Meacham, High toughness high hardness iron based PTAW weld materials, Materials Science and Engineering: A 428 (2006) 116–123.
[2] E. Badisch, M. Kirchgaßner, Influence of welding parameters on microstructure and wear behaviour of a typical NiCrBSi hardfacing alloy reinforced with tungsten carbide, Surface and Coatings Technology 202 (2008) 6016–6022.
[3] J.F. Flores, A. Neville, N. Kapur, A. Gnanavelu, An experimental study of the erosion-corrosion behavior of plasma transferred arc MMCs, Wear 267 (2009) 213–222.
[4] K. Van Acker, D. Vanhoyweghen, R. Persoons, J. Vangrunderbeek, Influence of tungsten carbide particle size and distribution on the wear resistance of laser clad WC/Ni coatings, Wear 258 (2005) 194–202.
[5] H.-J. Kim, S.-Y. Hwang, C.-H. Lee, P. Juvanon, Assessment of wear performance of flame sprayed and fused Ni-based coatings, Surface and Coatings Technology 172 (2003) 262–269.
[6] N.Y. Sari, M. Yilmaz, Improvement of wear resistance of wire drawing rolls with Cr–Ni–B–Si+WC thermal spraying powders, Surface and Coatings Technology 202 (2008) 3136–3141.
[7] H. Wang, W. Xia, Y. Jin, A study on abrasive resistance of Ni-based coatings with a WC hard phase, Wear 195 (1996) 47–52.
[8] W. Cerri, R. Martinella, G.P. Mor, P. Bianchi, D.D. Angelo, Laser deposition of carbide-reinforced coatings, Surface and Coatings Technology 49 (1991) 40–45.
[9] J. Nurminen, J. Näkki, P. Vuoristo, Microstructure and properties of hard and wear resistant MMC coatings deposited by laser cladding, International Journal of Refractory Metals and Hard Materials 27 (2009) 472–478.
[10] K.W.D. Hart, D.H. Harper, M.J. Gill, Case studies in wear resistance using HVOF, PTAW and Spray Fusion surfacing, in: 1st International Thermal Spray Conference, Materials Park, OH, ASM International, Montreal, Canada, 2000, pp. 1117–1125.
[11] A. Klimpel, A. Lisiecki, A. St. Klimpel, A. Rzeznikiewicz, Robotized GMA surfacing of cermetal deposits, Journal of Achievements in Materials and Manufacturing Engineering 18 (2006) 4.
[12] S. Babu, S. David, R. Martukanitz, K. Parks, Toward prediction of microstructural evolution during laser surface alloying, Metallurgical and Materials Transactions A 33 (2002) 1189–1200.
[13] R.C. Gassmann, Laser cladding with (WCW2C)/CoCrC and (WCW2C)/NiBSi composites for enhanced abrasive wear resistance, Materials Science and Technology 12 (1996) 691–696.
[14] C. Just, E. Badisch, J. Wosik, Influence of welding current on carbide/matrix interface properties in MMCs, Journal of Materials Processing Technology 210 (2010) 408–414.
[15] Q. Li, T.C. Lei, W.Z. Chen, Microstructural characterization of WCp reinforced Ni–Cr–B–Si–C composite coatings, Surface and Coatings Technology 114 (1999) 285–291.
[16] I.C. Grigorescu, C. Di Rauso, R. Drira-Halouani, B. Lavelle, R. Di Giampaolo, J. Lira, Phase characterization in Ni alloy-hard carbide composites for fused coatings, Surface and Coatings Technology 76–77 (1995) 494–498.
[17] V. Stoica, R. Ahmed, T. Itsukaichi, Influence of heat-treatment on the sliding wear of thermal spray cermet coatings, Surface and Coatings Technology 199 (2005) 7–21.
[18] S.W. Huang, M. Samandi, M. Brandt, Abrasive wear performance and microstructure of laser clad WC/Ni layers, Wear 256 (2004) 1095–1105.
[19] J. Przybylowicz, J. Kusinski, Structure of laser cladded tungsten carbide composite coatings, Journal of Materials Processing Technology 109 (2001) 154–160.
[20] N.P. Suh, Tribophysics, Prentice-Hall, New Jersey, 1986.
[21] T. Wolfe, Chemical and Materials Engineering, University of Alberta, Edmonton, Canada, 2010.
[22] E. Lassner, W.D. Schubert, TUNGSTEN: Properties, Chemistry, Technology of the Element, Alloys and Chemical Compounds, Kluwer Academic/Plenum Publishers, New York, 1990.
[23] T. Liyanage, G. Fisher, A.P. Gerlich, Influence of alloy chemistry on microstructure and properties in NiCrBSi overlay coatings deposited by plasma transferred arc welding (PTAW), Surface and Coatings Technology 205 (2010) 759–765.
[24] L.C. Lim, Q. Ming, Z.D. Chen, Microstructures of laser-clad nickel-based hardfacing alloys, Surface and Coatings Technology 106 (1998) 183–192.
[25] S. Bahadur, C.-N. Yang, Friction and wear behavior of tungsten and titanium carbide coatings, Wear 196 (1996) 156–163.
[26] J. Hu, D.Y. Li, R. Llewellyn, Synergistic effects of microstructure and abrasion condition on abrasive wear of composites – A modeling study, Wear 263 (2007) 218–227.
[27] M.J. Tobar, C. Álvarez, J.M. Amado, G. Rodríguez, A. Yáñez, Morphology and characterization of laser clad composite NiCrBSi–WC coatings on stainless steel, Surface and Coatings Technology 200 (2006) 6313–6317.